NUCLEAR SCIENCE AND ENGINEERING: **177**, 291–306 (2014)

Inventory Simulations Under Neutron Irradiation: Visualization Techniques as an Aid to Materials Design

M. R. Gilbert,* L. W. Packer, and J.-Ch. Sublet

EURATOM/CCFE Fusion Association, Culham Science Centre
Abingdon, OX14 3DB, United Kingdom

and

R. A. Forrest

International Atomic Energy Agency Nuclear Data Section
P.O. Box 100, 1400 Vienna, Austria

Received September 19, 2013
Accepted December 7, 2013
http://dx.doi.org/10.13182/NSE13-76

Abstract—*The simulation of neutron irradiation–induced transmutation using inventory codes is an important part of the research into materials in various nuclear environments, including fusion, fission, medical physics, nuclear security, and astrophysics. These simulations, even in their simplest form, such as the neutron irradiation of a single pure element, generate large time-dependent data sets of complex results. For each nuclide in the inventory, as a function of time, the output data will include the number of atoms and its contribution to a variety of radiological quantities including total or specific activity, gamma dose, heat output, and ingestion and inhalation hazards. A key challenge when performing inventory calculations is thus to represent the full complexity of the results in a visual and understandable format.*

This paper discusses two different approaches to visualizing inventory data: (a) nuclide maps, which allow the concentrations or activity contributions from all nuclides in the inventory to be displayed and also for the variation to be traced in time under a specific irradiation scenario, and (b) importance diagrams, which are a neutron spectrum–independent representation of the dominant nuclides that contribute to the activity of an irradiated material. Finally, these techniques are applied in parallel to investigate how the activation response of molybdenum can be improved via isotopic tailoring (enrichment or depletion), which could make it a more viable alternative armor material in the design of fusion reactors.

I. INTRODUCTION

Under neutron irradiation, materials undergo nuclear reactions causing a change in the nuclide composition (transmutation). Additionally, some of these newly created nuclides may be radioactive, leading to activation of the material. In nuclear fusion and in other industries where neutron fields are encountered—such as nuclear fission, astrophysics, nuclear security, or medical research—predicting, via simulation, the transmutation and hence activation response of materials is vitally important. Indeed, such calculations are often a necessary step to either satisfy regulators (in the case of the nuclear power industries) or define acceptable working limits (exposure times, maximum concentrations, etc.) for a given material. In fusion research, because of a lack of a working power plant or experimental reactor, or a fully representative neutron irradiation materials testing facility, calculated predictions are currently the primary tool used to guide engineers and designers in the planning of future reactors and the associated choice of materials.

*E-mail: mark.gilbert@ccfe.ac.uk

Typically, predicting the transmutation response of materials to a specific neutron irradiation field, perhaps measured in a reactor or simulated using neutron transport codes such as MCNP (Refs. 1 and 2), requires an inventory code that numerically solves a set of coupled differential equations—one for each possible nuclide—that cannot generally be solved analytically except under special circumstances (see Ref. 3, for example). The inventory code uses these equations to evolve the nuclide composition in time both during irradiation and afterward, as the generated radionuclides decay to stable alternatives. For one nuclide, the differential equation is

$$\frac{dN_i}{dt} = \underbrace{-N_i(\lambda_i + \sigma_i\phi)}_{loss} + \sum_{j \neq i} \underbrace{N_j(\lambda_{ji} + \sigma_{ji}\phi)}_{creation} , \qquad (1)$$

where N_i is the number of atoms of nuclide i at a given time t and the *loss* term has λ_i as the decay constant of the nuclide, ϕ as the total neutron flux ($n \cdot cm^{-2} \cdot s^{-1}$), and σ_i as the total collapsed cross section for all possible reactions on the nuclide (measured in barns and calculated by combining the energy-dependent specified neutron field with nuclear reaction cross-section data). The corresponding *creation* term in Eq. (1) is the sum over all other nuclides with the *ji* subscripts indicating the production of nuclide i from a reaction or decay on j. Note that in this formulation the contributions to creation and loss from fission reactions are included in the σ_{ji} and σ_i terms, respectively.

Even in the simplest of cases, these equations can lead to an initially small list of nuclides present in the inventory, such as those making up the natural abundance of a single pure element, to quickly grow much larger under irradiation. Analyses involving global quantities representing the evolution of the whole sample, such as total activity or total decay heating, can be easily displayed graphically. However, this hides much of the complexity inherent to the results, which can often only be inferred or described briefly. Thus, one of the main goals of the present work was to develop methods of visualization that give as much detail as possible, while still being understandable to both specialists in nuclear physics and to those applying the findings, who may not otherwise appreciate how complex the response of a material to neutron irradiation can be.

This paper describes two alternative and complementary visual representations of the results from inventory calculations. Later, we will reintroduce importance diagrams, originally developed by Forrest[4] and now updated and extended using the latest computational and graphical tools, which show the activation response of a material after neutron irradiation in terms of dominant radionuclides. First, however, we discuss a method to show either the transmutation or activation response of a material under a given neutron irradiation field in a nuclide map. Finally, an application of the two techniques will be demonstrated by considering the isotopic contributions to the response of molybdenum (Mo).

All of the results presented were obtained with the recently released FISPACT-II inventory code[5] using the latest TALYS-based Evaluated Nuclear Data Libraries[6,7] (TENDL), which are both part of the EASY-II European Activation SYstem.[8]

II. NUCLIDE MAPS

Under a specific neutron irradiation field, the variation in concentration due to transmutation as a function of time can be plotted straightforwardly at the elemental level, as is shown in Fig. 1 for the burnup of pure tungsten (W) during a 5–full-power-year (FPY) irradiation in a typical DEMO first-wall environment (DEMO is the planned next-step demonstration fusion power plant; see Gilbert et al.[9] for details of the model used and resulting neutron

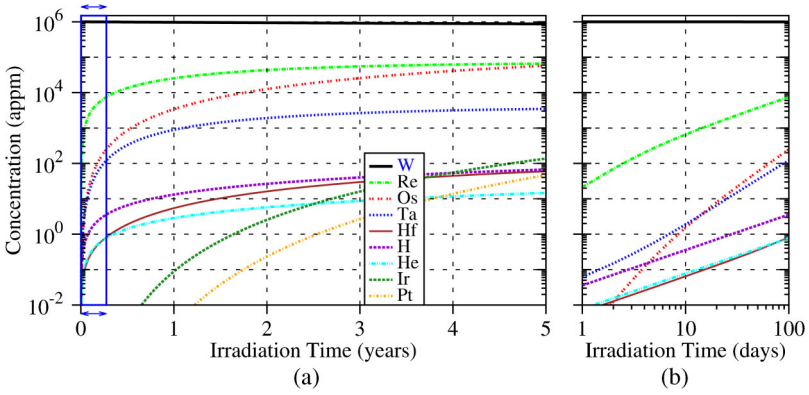

Fig. 1. Transmutation response at the elemental level of pure W during a 5-FPY irradiation in DEMO first-wall conditions.[9] The concentration of each element produced under irradiation is given in appm. The full 5-FPY evolution on a linear timescale is shown in (a), while the reduced plot of (b) shows, on the same concentration scale, the evolution from 1 to 100 days [indicated by the arrows and box in (a)] on a logarithmic timescale for direct comparison with Fig. 2.

spectra). However, such plots quickly become too complicated if one attempts to separate out the variation as a function of individual nuclides.

As an alternative, a process has been developed to represent the full complexity of a transmutation calculation by showing the nuclides on a so-called nuclide map, where nuclides are presented in a tableau with atomic number Z of the parent element increasing vertically and the neutron number N of the nuclide increasing horizontally. A color gradient is then used to represent the concentration in atomic parts per million (appm) of each nuclide. The variation with time can be subsequently appreciated by animating these maps with snapshots in time. A computer code, written in FORTRAN, has been created to automatically analyze the results from a given FISPACT-II output file and write the necessary command statements to produce the sequence of nuclide map snapshots with the freely available GNUPLOT plotting program.[10]

The ability to produce animations showing the buildup (and decay) of different nuclides during (and after) irradiation is the main strength of this approach; however, in this paper, only sequences of snapshots are shown. Figure 2 shows such a sequence of snapshots in time for the same irradiation calculation depicted in Fig. 1. Note that while it is conceivable to plot all possible nuclides on a single chart, of which there are 3873 in the decay file associated with the latest release of EASY-II (Ref. 8), it is more convenient to focus on those regions containing the nuclides in the inventory being analyzed. Thus, Fig. 2 shows only the region of the map near W ($Z=74$), as well as the low-Z part ($Z=1, 2, 3$) to highlight the fact that gas nuclides of helium and hydrogen are also produced. In a more complex simulation, such as in the irradiation of a steel alloy, it may be necessary to display a number of important regions simultaneously. The current version of the computer code used to produce these maps is able to plot user-defined subregions of the full nuclide chart, and multiple plots can be shown side by side or, as in plots shown here, embedded in the same image using extra scripting routines and the multiplot option within GNUPLOT (Ref. 10).

Figure 2 shows how the initial inventory at time zero, which was made up of the naturally occurring isotopes of W in their appropriate relative abundances, changes dramatically during the course of the irradiation. The inventory spreads across the nuclide map as time progresses, reaching (under the chosen color gradient) as far as ^{194}Pt in increasing atomic mass (^{195}Pt is also just starting to appear) and down to ^{178}Hf in decreasing atomic mass. As is observed in Fig. 1, a number of other elements are produced during the irradiation, but the nuclide map makes it possible to observe which particular isotopes (of an element) are the main contributors to the composition. For example, while osmium (Os) is produced in significant quantities during the irradiation, the nuclide maps show that neither of the main isotopes of naturally occurring Os, ^{192}Os (40.78% abundance) and ^{190}Os (26.26%), are produced in large concentrations. Rather, it is ^{188}Os that dominates, reaching almost 40 000 appm (or 4 at. %) by the end of the 5-FPY irradiation, followed by ^{186}Os at 7600 appm.

The variation in concentration of nuclides during an irradiation can also be extended beyond shutdown to observe how the inventory decays to a stable configuration as radionuclides disappear (as a function of their half-lives) and increases the concentrations of stable nuclides. However, it is also useful to apply the same techniques to show instead how radionuclides contribute to the various radiological quantities that are calculated during inventory calculations. On such maps, the stable nuclides are always white, unless they have important metastable states that generate significant activity, which are designated by an m on the maps.

Figure 3 shows a sequence of snapshots depicting the variation in gamma dose rate, measured in sieverts per hour, of the same 1-kg sample of pure W irradiated under the same DEMO first-wall conditions as before. In fusion power plant conceptual designs, W is the primary candidate material for the divertor armor of reactors, which is a component that will require maintenance or replacement at regular intervals of 5 yr or less, and so, the gamma dose rate will be a critical measure determining the acceptable handling procedures. Note that the same subregions of the nuclide map used for Fig. 2 are also used here, even though none of the gas radionuclides contribute to the gamma dose. The first snapshot in this case is immediately after the 5-FPY irradiation, when the total dose rate in the sample is 1.45×10^{5} Sv·h^{-1} (as shown in the snapshot). A very large number of nuclides contribute to the total dose rate, although ^{187}W (1.1×10^{5} Sv·h^{-1}) dominates, followed by ^{182}Ta (2.0×10^{4}) and ^{188}Re (9.7×10^{3}). In subsequent snapshots, the dose rate contributions after different amounts of cooling are shown, illustrating how different nuclides become dominant as others decay away. After 10 yr of cooling, the total dose rate has fallen by nine orders of magnitude, and there are only a few nuclides still contributing, while after 1 million yr of cooling (final snapshot in Fig. 3), only two nuclides show any significant contribution at all. One of these, ^{186}Re, includes a dominant contribution from ^{186m}Re, which has a very long half-life ($T_{1/2}=2\times10^{5}$ yr), and a smaller but still significant contribution from the short-lived ($T_{1/2}=3.72$ days) ^{186}Re ground state to which it decays. The other contributing nuclide, ^{182}Ta, is present despite its relatively short half-life ($T_{1/2}=114.43$ days) because ^{182}Hf (which produces a very little gamma dose and so appears white in the maps) β^{-} decays to it and has a very long half-life of 9×10^{6} yr.

The analysis above illustrates one potential application of these nuclide maps, namely, the ability to identify the set of problem radionuclides for a given radiological quantity. This concept is explored further in Sec. IV.

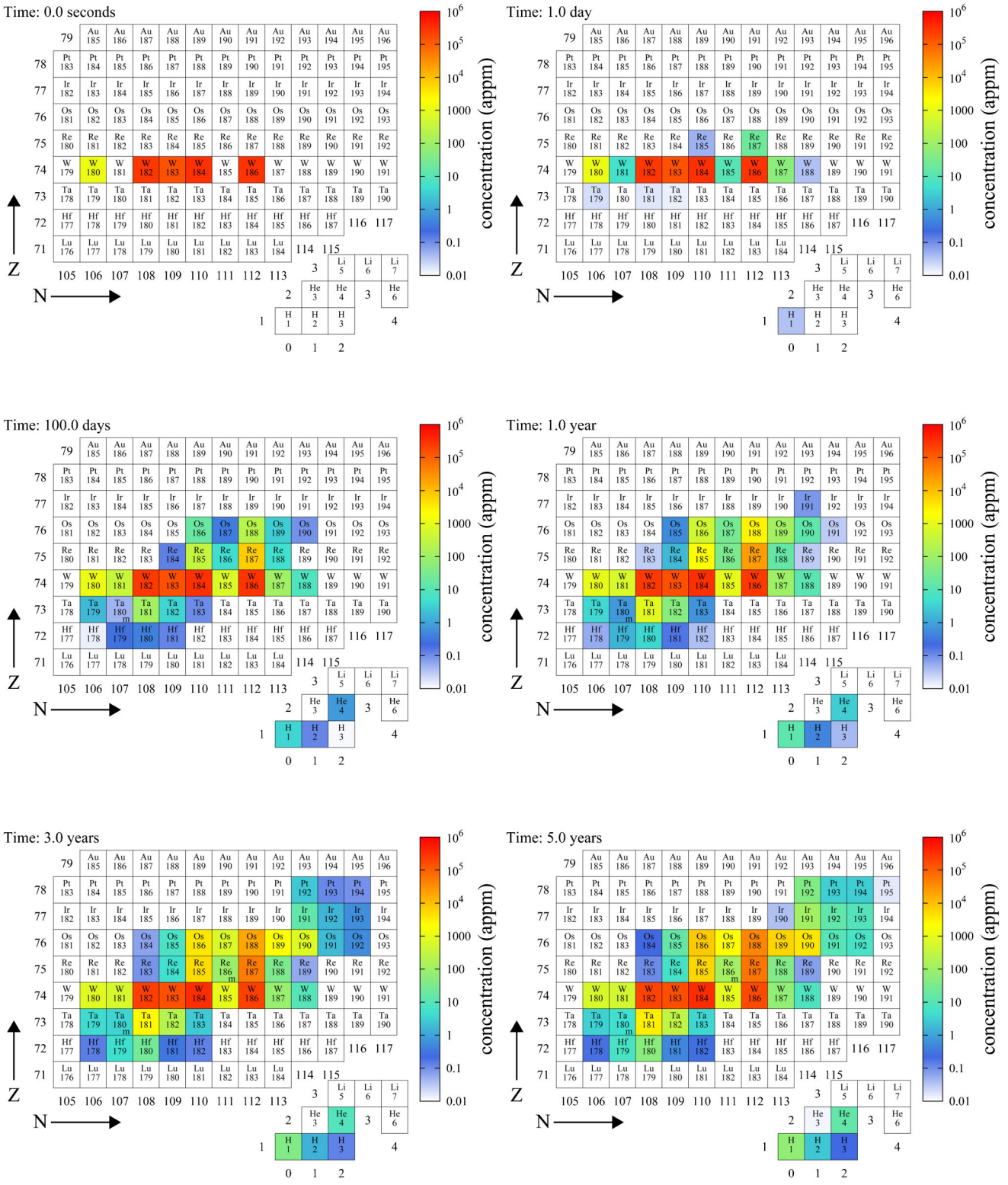

Fig. 2. A sequence of nuclide maps showing the change in composition of initially pure W during a 5-FPY irradiation under DEMO first-wall armor conditions with a total neutron flux of 8.25×10^{14} n·cm^{-2}·s^{-1} (see Ref. 9 for more details). An *m* in the box of a particular nuclide indicates that the primary contribution to the concentration comes not from the ground state nuclide but from one or more of its excited or *m*etastable states.

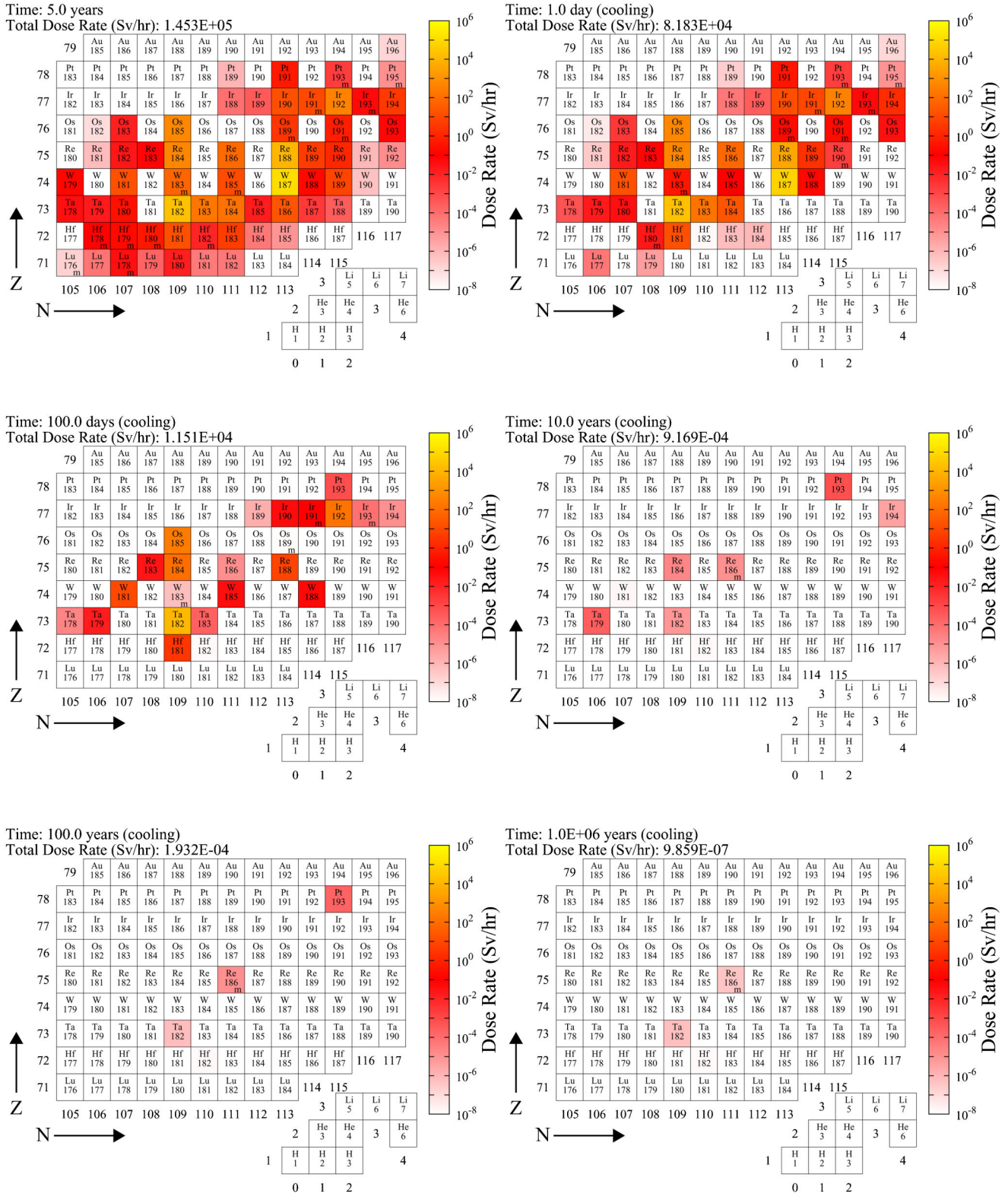

Fig. 3. A sequence of nuclide map snapshots showing the variation in gamma dose rate contributions during up to 1 million yr of cooling after the 5-FPY irradiation in DEMO first-wall conditions. An *m* in the box of a nuclide indicates that the primary contribution to dose rate comes from the nuclide in an excited or *m*etastable state.

III. IMPORTANCE DIAGRAMS

Importance diagrams were first developed by Forrest[4] in the late 1990s, with the specific goal of finding a technique to visualize the general, neutron field–independent post-irradiation activation response of a material. Full details of these diagrams are given in Ref. 4, but they are described briefly here. Importance diagrams show the regions of the decay time versus incident neutron energy plane that are dominated by one radionuclide, i.e., where a nuclide contributes $>50\%$ of the radiological quantity considered at a given neutron energy and cooling time. Diagrams can be created for any calculated radiological quantity, including specific or total activity, measured in disintegrations per second (becquerels); gamma dose rate, measured in sieverts per hour; or decay heat output, measured in kilowatts.

The first step in the creation of importance diagrams for a specific material is a series of inventory calculations, one for each incident neutron energy of a specific energy group structure (see Ref. 5 for details of the different group structures available in FISPACT-II). Each calculation should have identical irradiation conditions and identical cooling time intervals. Subsequently, these inventory results must be analyzed to identify regions of the decay time–neutron energy space where one radionuclide dominates the radiological response of the input material, which can then be plotted on a contour map. Note that the 50% dominance threshold leads to some areas of an importance diagram being empty because no single nuclide dominates, and in such cases further analysis of the inventory results is required to identify important nuclides.

Previously, the creation of importance diagrams using the forerunner of FISPACT-II (known as FISPACT), relied on using a Microsoft Windows–based graphical user interface in conjunction with proprietary plotting software to create the contours of dominance. Unfortunately, this limited the use of the diagrams as users either did not have the required plotting software or were using Unix-based operating systems. A notable exception is the so-called Activation Handbook, of which Ref. 11 is the latest version, which presents importance diagrams for various radiological quantities of all naturally occurring elements. To resolve these issues, a code has been written in FORTRAN, which means it is as portable as FISPACT-II itself, which will prepare the necessary batch scripts and FISPACT-II input files to automate the inventory calculations and then subsequently read the results, define the contours associated with dominant nuclides, and write the necessary command statements to produce the contour maps [in the present case using the freely available GNUPLOT (Ref. 10)]. Note that the importance diagram routines developed in this work will be incorporated into future releases of the EASY-II code system, making the only additional requirement for users the need to have a suitable two-dimensional plotting program, of which there are several freely available.

A by-product of this new more flexible approach to producing importance diagrams is that their capabilities and applications can now be expanded. In particular, the new computer code can read in the large set of FISPACT-II results (typically containing 709 separate files; see below in Sec. III.A) and produce importance restart files that can be subsequently reprocessed as many times as required to fit a particular purpose. Some of the features that arise as a natural consequence of the new flexibility are highlighted below by considering the activation response of fusion-relevant materials.

III.A. Resolution and Energy Range Enhancements

The level of detail depicted in an importance diagram is highly dependent on the choice of resolution in both the neutron energies and decay times. A key benefit of the new developments discussed above is the ability to process results in higher-resolution neutron energy group structures or, indeed, finer decay time intervals.

In Ref. 4 and throughout the short history of importance diagrams, the energy group structures used have been relatively coarse, often containing only 175 energy bins (or even just a small subset of these) to cover a wide range of fusion-relevant neutron energies from a few hundredths of an electron volt up to >14 MeV. This was partially caused by the unavailability of nuclear data in finer group structures for inventory calculations but was also a response to the somewhat slower computational speed of the original FISPACT inventory code (FISPACT-II is around $3\times$ faster with the same data libraries). Furthermore, the interface between the inventory results and plotting software was somewhat cumbersome, requiring the transfer of the raw data into a spreadsheet, which could then be analyzed by the plotting software to produce the contours. The new code performs all of the reading and processing in one step, and the plotting software merely has to plot the defined contours.

The latest TENDL-based neutron libraries distributed with EASY-II have a fine 709-bin (Ref. 5) group structure, 650 bins of which cover the same energy range of 1×10^{-5} eV to 20 MeV of the previously used 175-bin group structure. Since the difference in computation speed between using this 709-bin grid or a much coarser grid to generate importance diagrams is only minor, this fine grid has been used throughout the present work. This has been combined with a fine decay time grid containing ten equally spaced intervals for every order of magnitude in time measured in seconds, which gives around 120 intervals covering cooling times from 0 to 3.2×10^{13} s compared to fewer than 30 intervals used in previous calculations.[4]

Figure 4a shows the total or specific activity importance diagram for pure W irradiated for 5 yr at a neutron flux in each energy bin of 1×10^{15} n·cm^{-2}·s^{-1},

which is the peak flux expected in the first-wall environment of fusion reactors.[9] The fine energy grid allows a clearer observation of the effect of the resonances in the neutron capture (n,γ) cross sections of the various isotopes of W (see Ref. 12 for more details). Previously, with the coarse energy group structure, only the influence of broad, isolated resonances was observable, such as the resonance at 132 eV in the ^{59}Co$(n,\gamma)^{60}$ Co cross section,[4] but now, even narrow resonances are resolved. At a given resonance energy, there is a pronounced increase in the production of certain radionuclides, causing them to be dominant over a wider range of decay times. This produces narrow horizontal bands of dominance for these radionuclides that extend below (in decay time) their main regions of dominance. For example, ^{185}W has these horizontal bands due to the resonance in the capture cross section of ^{184}W, which is the most abundant naturally occurring isotope of W (30.64% abundance).

Meanwhile, Fig. 4b highlights the flexibility of the new processing system as it demonstrates how the axes of the plots can be adapted to suit specific needs. The plot shows the same result as in Fig. 4a, but this time the upper portion of the energy axis, above 5 MeV, is shown on a linear scale. This allows the important nuclides associated with an energy of $\sim$14 MeV, which is the energy of neutrons produced in the deuterium-tritium fusion reaction, to be better appreciated. In subsequent sections (from Fig. 6, Sec. III.B onward), this split axis scale with a range from 0.06 eV to 30 MeV has been used throughout.

As well as the finer group structures, the TENDL libraries used here also have a greatly extended range compared to the mostly fusion-specific nuclear data used previously. In particular, the 709-group structure extends down to 1×10^{-5} eV and up to 200 MeV (2×10^{8} eV), with theoretical extensions up to 1 GeV (1×10^{9} eV). Figure 5 compares the heat output (measured in kilowatts) importance diagram for pure copper (Cu) with this extended incident neutron energy range to one using the standard range discussed above. In the extended range (Fig. 5b), an extra nine nuclides have dominant regions in the importance diagram.

III.B. Variation with Irradiation Scenario and Material Composition

Another valuable feature available with the new processing is the ability to specify the list of nuclides to be plotted in the importance diagram and, hence, the order in which they appear. This, in particular, allows several similar importance diagrams to be plotted with a fixed nuclide list, enabling direct comparison as a function of some varying parameter or parameter set. As with the nuclide maps discussed earlier, this provides for the possibility of generating animated importance diagrams, especially given the relative ease with which multiple diagrams can now be created.

Figure 6 shows a sequence of ingestion dose (measured in Sv·kg^{-1} as the dose received by an average person over a 50-yr period per mass of ingestion) importance diagrams for pure iron (Fe) where the varying parameter is the irradiation time (given in the top right-hand corner of each plot). As the irradiation time increases, certain nuclides become more dominant while the importance of others reduces. For example, after a 1-h irradiation of pure Fe, both ^{56}Mn and ^{59}Fe dominate at short decay times over most of the neutron energy range, but after a 5-yr irradiation, they have largely been superseded by ^{55}Fe. In this particular scenario, it is also

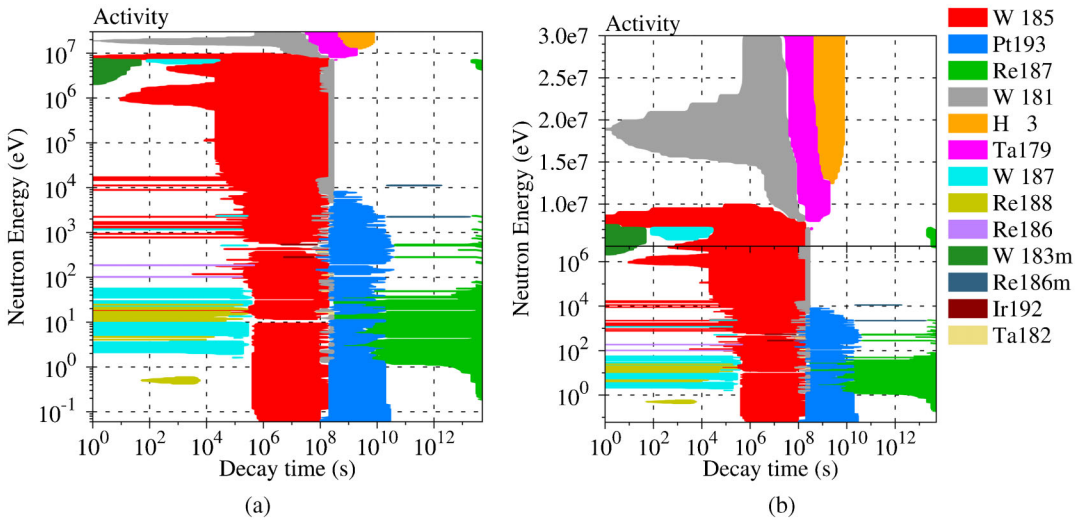

Fig. 4. Specific activity importance diagrams for pure W irradiated for 5 yr at a flux of 1×10^{15} n·cm^{-2}·s^{-1}. In (a) the neutron energy axis is logarithmic, while in (b) there is a split at 5×10^{6} eV with a logarithmic scale below down to 0.06 eV and linear scale above up to 30 MeV.

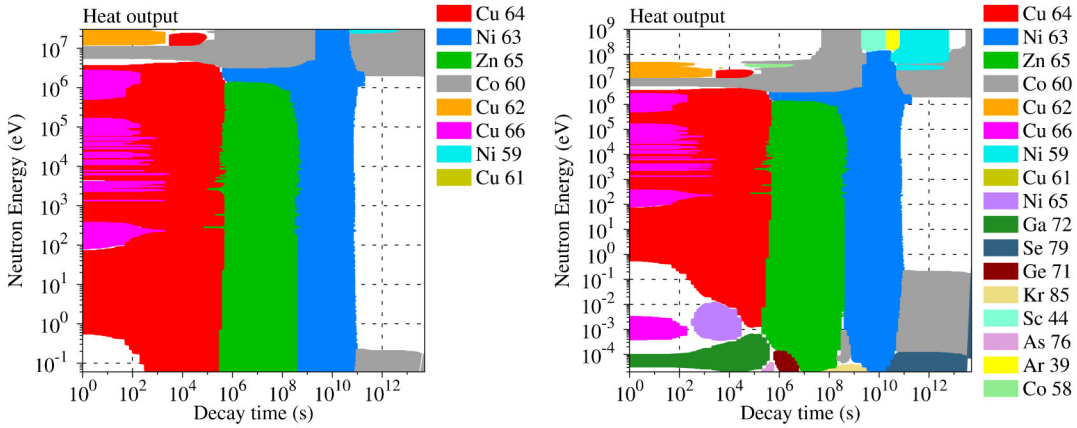

Fig. 5. Heat output (or decay heat) importance diagrams for pure Cu irradiated for 5 yr at a flux of 1×10^{15} n·cm^{-2}·s^{-1}. The standard 0.06-eV to 30-MeV range is shown in (a), while (b) demonstrates the extra nuclides that appear when the full energy range of 1×10^{-5} eV to 1 GeV available in the latest TENDL libraries is used.

worth noting that two nuclides of argon (Ar) start to appear at high neutron energies (above 6 MeV) at the longer irradiation times, which is a reflection of the fact that more transmutation has taken place leading to the possibility of longer and longer reaction pathways.

It is also possible to investigate the influence of neutron flux on the dominant nuclides. Figure 7 shows a sequence of gamma dose rate importance diagrams for pure W, irradiated for 5 yr, with the neutron flux used in each monoenergetic inventory calculation varying from 1×10^{10} to 1×10^{16} n·cm^{-2}·s^{-1}. In contrast to the findings in Ref. 4, there are some striking differences among the diagrams. At low irradiation fluxes the importance diagrams are dominated by a relatively small number of radionuclides, with, for example, only five nuclides, ^{187}W, ^{182}Ta, ^{179m}Hf, ^{181}W, and ^{179}Ta, covering the majority of the energy-decay-time plane when the irradiation flux is only 1×10^{10} n·cm^{-2}·s^{-1} (there are also two minor regions associated with ^{185}W and ^{181}Hf). The number of dominant nuclides increases significantly with flux, and correspondingly, the size of the dominant regions decreases, so that by 1×10^{16} n·cm^{-2}·s^{-1} there are 15 nuclides with dominant regions in the diagram (note that there are 20 nuclides in the Fig. 7 legend because some nuclides show dominance only at lower fluxes). Furthermore, the dominant nuclides that cover the largest fractions of the importance diagram change. For example, the regions dominated by ^{182}Ta (at high neutron energy) shrink dramatically, and at the highest fluxes it is generally only important at longer decay times. As the flux increases still further, beyond what is shown in Fig. 7, the number of nuclides contributing to the dose becomes so great that the importance diagram becomes largely empty as very few nuclides reach the >50% dominant level.

Finally, and perhaps most relevantly for material design, it is possible to observe the variation in importance diagrams as a function of input material composition. The previous cases discussed above have been restricted to the importance diagrams of pure elemental materials, but there is no reason why this should be so—the input material can be made up of multiple elements (see, for example, importance diagrams of Type 316 stainless steel depicted in Ref. 4 or of the fusion-specific Eurofer-97 in Ref. 13). Figure 8 shows a sequence of heat output importance diagrams for varying compositions of a simple iron-nickel (Fe-Ni) binary alloy. Such a study has relevance to fusion research as both Type 316 stainless steel (dominated by Fe but containing ~10% Ni) and INCONEL® alloy 718[a] (~50% Ni, but with >20% Fe) are major structural alloys used in the conceptual designs of future power reactors, such as DEMO, and in the plans for the under-construction experiment called ITER (Ref. 14). Note that chromium (Cr) is also a major component of these two alloys, but in this simple parameter study it is omitted.

Figure 8 shows that as the concentration of Ni increases, the main radionuclides of Fe (^{55}Fe and ^{59}Fe) are largely replaced by equivalent radionuclides of Ni, including ^{65}Ni, ^{59}Ni, and ^{63}Ni. Even at a low Ni concentration of only 5 wt%, the long-lived ^{59}Ni ($T_{1/2} = 7.6 \times 10^4$ yr) dominates the heat output at long timescales (above 10^{11} s, corresponding to ~3000 yr), while the shorter-lived ^{63}Ni ($T_{1/2} = 101$ yr) immediately dominates at all neutron energies on the 10^9- to 10^{10}-s timescale (~30 to 300 yr). This illustrates the fact that Ni is problematic under neutron irradiation, which is why its

[a]INCONEL is a registered trademark of the Special Metals Corporation group of companies.

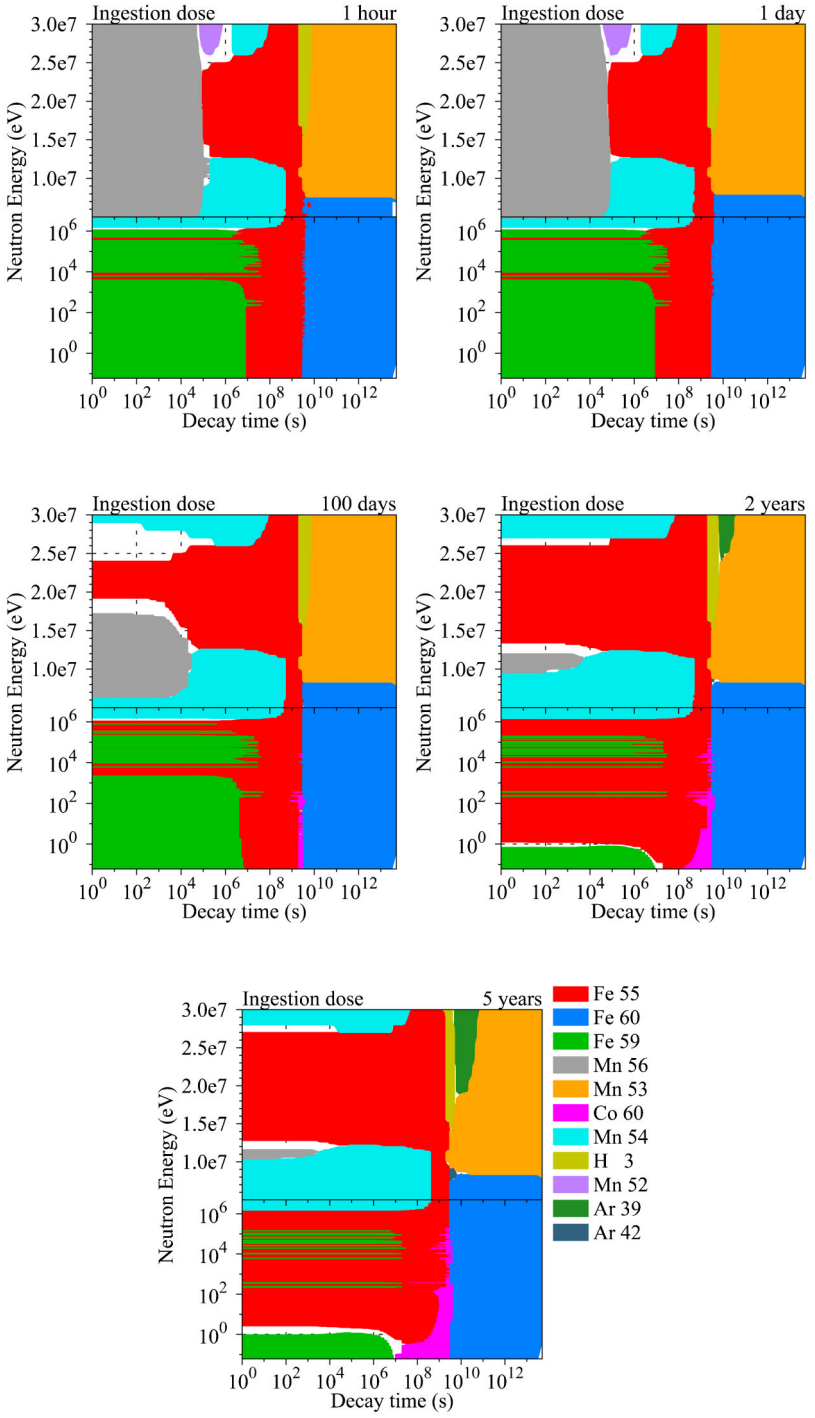

Fig. 6. Variation in the ingestion dose importance diagram of pure Fe as a function of irradiation time at a fixed flux of 1×10^{15} n·cm^{-2}·s^{-1}. The irradiation times (shown above each plot) vary from 1 h up to 5 yr, and the same nuclide coloring (see the legend) is used in all diagrams.

content in near-plasma components of fusion reactors must be carefully controlled.

Meanwhile, ^{60}Co is important in all the diagrams, which is no surprise given the position of cobalt between Fe and Ni in the periodic table. However, as the Ni content increases, other Co radionuclides appear in the diagrams, with, in particular, ^{58}Co largely replacing ^{56}Mn at short cooling times.

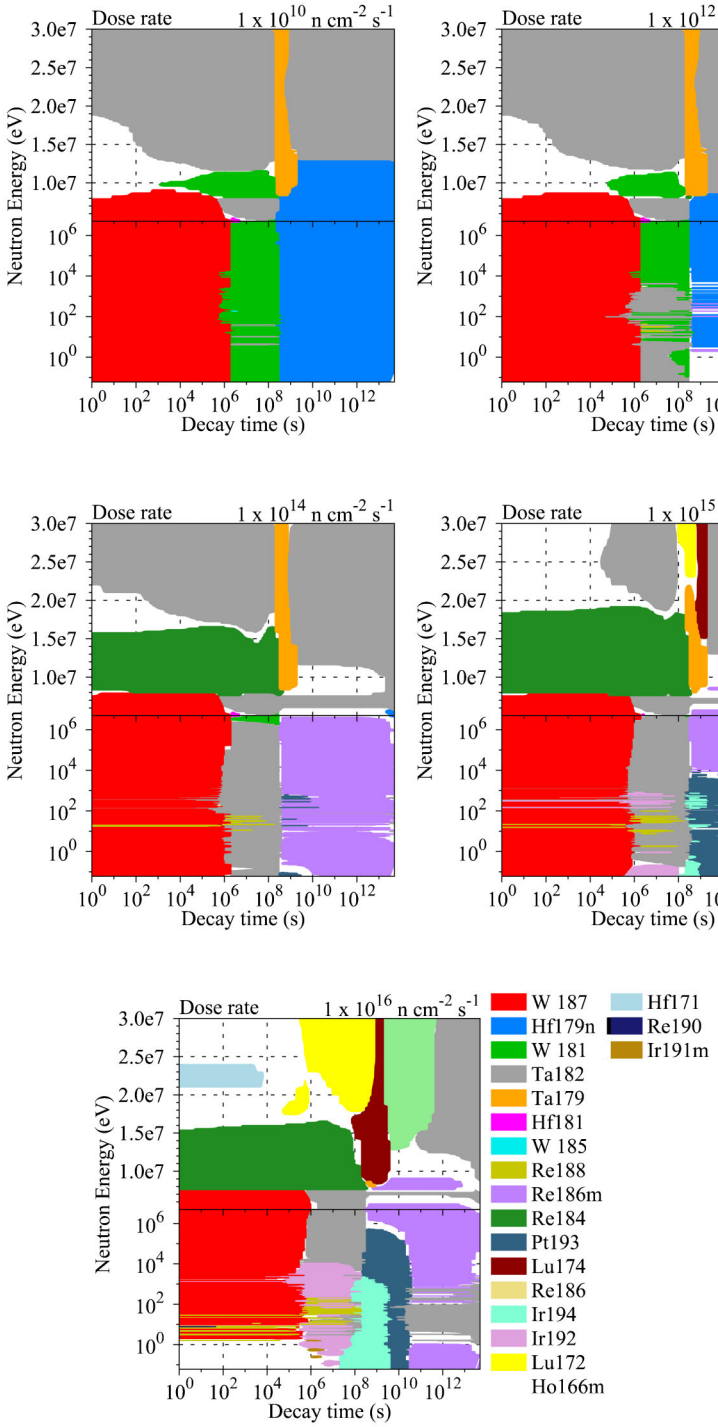

Fig. 7. Variation in gamma dose rate importance diagrams for pure W as a function of irradiation flux after a 5-yr irradiation. The irradiation fluxes (shown above each plot) vary from 1×10^{10} to 1×10^{16} n·cm^{-2}·s^{-1}.

IV. CASE STUDY: ISOTOPIC TAILORING (ENRICHMENT OR DEPLETION) OF MOLYBDENUM

In Secs. II and III two different methods for visualizing and interpreting the results of inventory calculations were discussed. In what follows, the activation of Mo is investigated to illustrate the potential applications of using the two techniques in parallel.

Molybdenum is often discussed as a possible alternative to W as a first-wall and divertor armor material

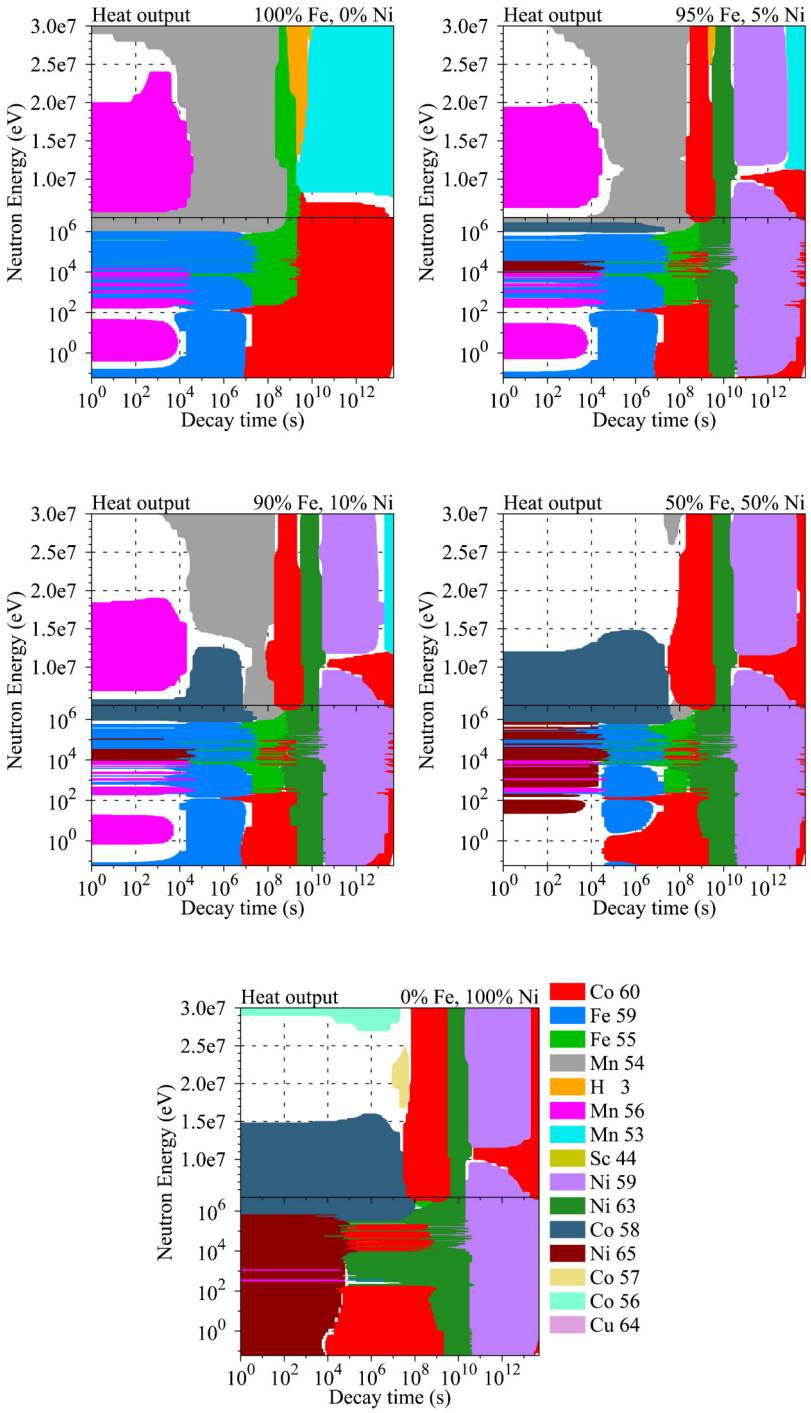

Fig. 8. A sequence of heat output importance diagrams for varying compositions of the binary alloy Fe-Ni after 5-yr irradiations at a flux of 1×10^{15} n·cm^{-2}·s^{-1}. The weight percentages of Fe and Ni in each composition are shown at the top right-hand corner of each diagram.

in fusion reactors because of its similar characteristics, such as high melting point [2896 K in Mo compared to 3695 K in W (Ref. 15)] and good thermal conductivity (138 versus 174 W·m^{-1}·K^{-1} at room temperature[15]) and its potential to negate some of the problems with W, including fabrication difficulties and embrittlement under irradiation. Mo could also be used as a substrate material onto which W could be bonded, thus helping to resolve the mismatch between the operating temperatures of W and the structural steels beneath. However, there is

currently a barrier to the use of Mo because under neutron irradiation it produces long-lived radioactive isotopes. This leads to levels of activity at timescales on the order of hundreds of years that are significantly higher than either W or the fusion-baseline material Fe. For example, in Fig. 9—which shows how the gamma dose rate in Mo, after a 5-FPY irradiation in a typical DEMO spectrum, decays with time compared to the equivalent results in W and Fe—it is clear that the gamma dose from Mo remains high beyond 100 yr of cooling.

The reasons for this long-lived activation can be investigated using nuclide maps of the dose rate as a function of cooling time. Figure 10 shows eight nuclide maps for the same DEMO first-wall irradiation of pure Mo as used in Fig. 9. Six of these give the variation in nuclide contributions to the gamma dose rate as a function of cooling time, starting from the position at zero cooling time, immediately after shutdown (labeled in Fig. 10 as a time of 5 yr). As seen previously with W, initially a large number of radionuclides contribute to the dose rate, with particularly high contributions from ^{101}Mo (2.9×10^4 Sv·h^{-1}) and ^{99}Mo (1.3×10^4 Sv·h^{-1}). However, many of these nuclides have relatively short half-lives (^{101}Mo is particularly short-lived with $T_{1/2} = 14.61$ min), and so, as the cooling time increases, the number of contributing nuclides falls dramatically. After 100 yr, there is only a handful of nuclides, and after 100 000 yr, only three nuclides, ^{94}Nb, ^{98}Tc, and ^{92}Nb, with half-lives of 2×10^4, 4.2×10^6, and 3.5×10^7 yr, respectively, show any significant contribution to the dose rate. In the crucial

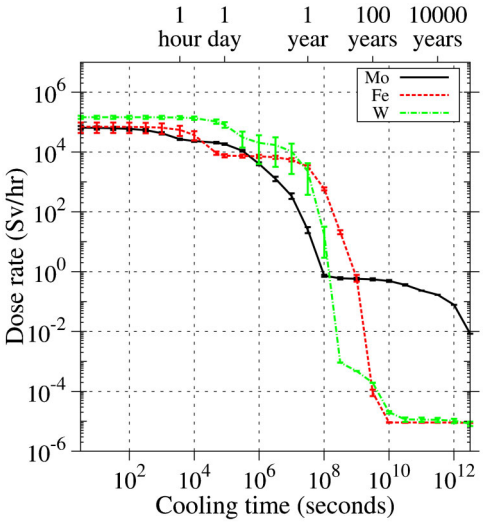

Fig. 9. The variation in gamma dose rate during cooling after a 5-FPY irradiation of 1 kg of Mo, W, and Fe under a DEMO outboard equatorial first-wall armor spectrum with a total flux of 8.25×10^{14} n·cm^{-2}·s^{-1} (see Ref. 9 for details). The error bars on each curve are due to defined uncertainties in the nuclear data. The straight lines connecting adjacent data points serve as a guide to the eye only.

period, between ~100 and 10 000 yr (see Fig. 9), note that the primary contributor to the dose rate is ^{94}Nb and, to a lesser extent, ^{91}Nb ($T_{1/2} = 700$ yr).

How can the activity generated by these long-lived nuclides be mitigated? The initial concentration nuclide map in Fig. 10 (the second concentration map gives the shutdown composition, which once again demonstrates the large inventory of nuclides created under irradiation) shows that Mo has a relatively large number (seven) of stable isotopes making up its naturally occurring composition. This immediately suggests that isotopic tailoring, where the natural isotopic abundances are altered via enrichment or depletion to meet some application requirement, could be applied to Mo. In the fission industry, for example, uranium (U) is enriched in ^{235}U to improve reactor efficiency, while Sublet and Butterworth[16] previously considered the isotopic tailoring of titanium (Ti) for fusion applications. Even more advantageously, the natural abundances of Mo's isotopes are all at a similar level, ranging from 9.25% (^{94}Mo) to 24.13% (^{98}Mo); i.e., the composition is not dominated by one nuclide (as in Fe with ^{56}Fe: 91.754% abundance) and contains no negligible isotopes that would be difficult to enrich (as in W with ^{180}W at only 0.12%).

To discover if isotopic tailoring could be beneficial to the overall activation of Mo, we consider the gamma dose rate importance diagrams of each of its isotopes (FISPACT-II allows for specific nuclide compositions as the starting material, not just particular elemental concentrations; see Ref. 5 for details). In particular, these will help to identify if particular isotopes are responsible for the creation of the "problem" radionuclides highlighted above. Figure 11 shows the set of gamma dose rate importance diagrams for the seven naturally occurring isotopes of Mo. For each isotope diagram, a sequence of 709 inventory calculations was performed with 1 kg of the isotope (meaning that the number of initial atoms decreases slightly with increasing isotope mass) with 5-yr irradiations.

From Fig. 11, note that there are large differences between the importance diagrams, especially when comparing the lighter isotopes with the heavier ones. For example, the diagram for ^{92}Mo has dominant regions for 11 different radionuclides, while for ^{100}Mo there are 12, and there are only 3, ^{93m}Nb, ^{95}Nb, and ^{94}Nb, that appear in both, and even then the regions where these three nuclides are dominant are completely different. For the lightest stable isotope, ^{92}Mo, these three overlapping radionuclides are dominant only in low neutron energy regions because they are produced via neutron capture reactions on ^{92}Mo, and the cross sections of such reactions increase with decreasing neutron energy. Meanwhile, for the heaviest isotope, ^{100}Mo, these same three nuclides are created by reactions involving neutron capture followed by emission of a light charged particle, such as an alpha particle. Reactions of this kind often have thresholds and certainly have significant cross sections only at high

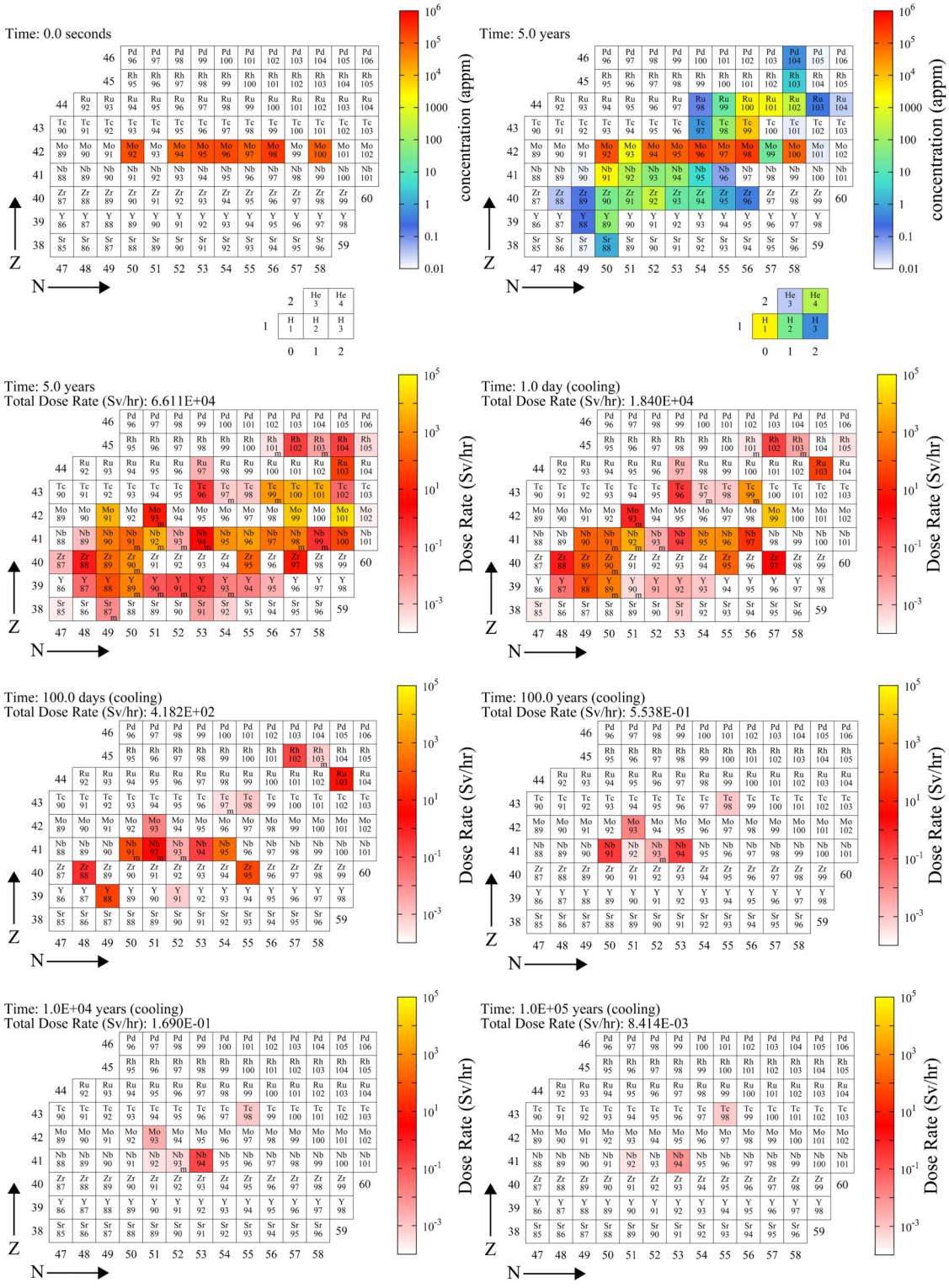

Fig. 10. Nuclide maps as a function of time in pure Mo: two, with a blue-green-yellow-red color scale, showing the initial and final concentrations of the nuclides resulting from a 5-FPY irradiation in DEMO first-wall conditions (the same used in Fig. 9), and then six, with a red-orange-yellow scale, showing how the different transmutant nuclides contribute to the gamma dose rate as a function of cooling time, starting from the situation immediately upon shutdown.

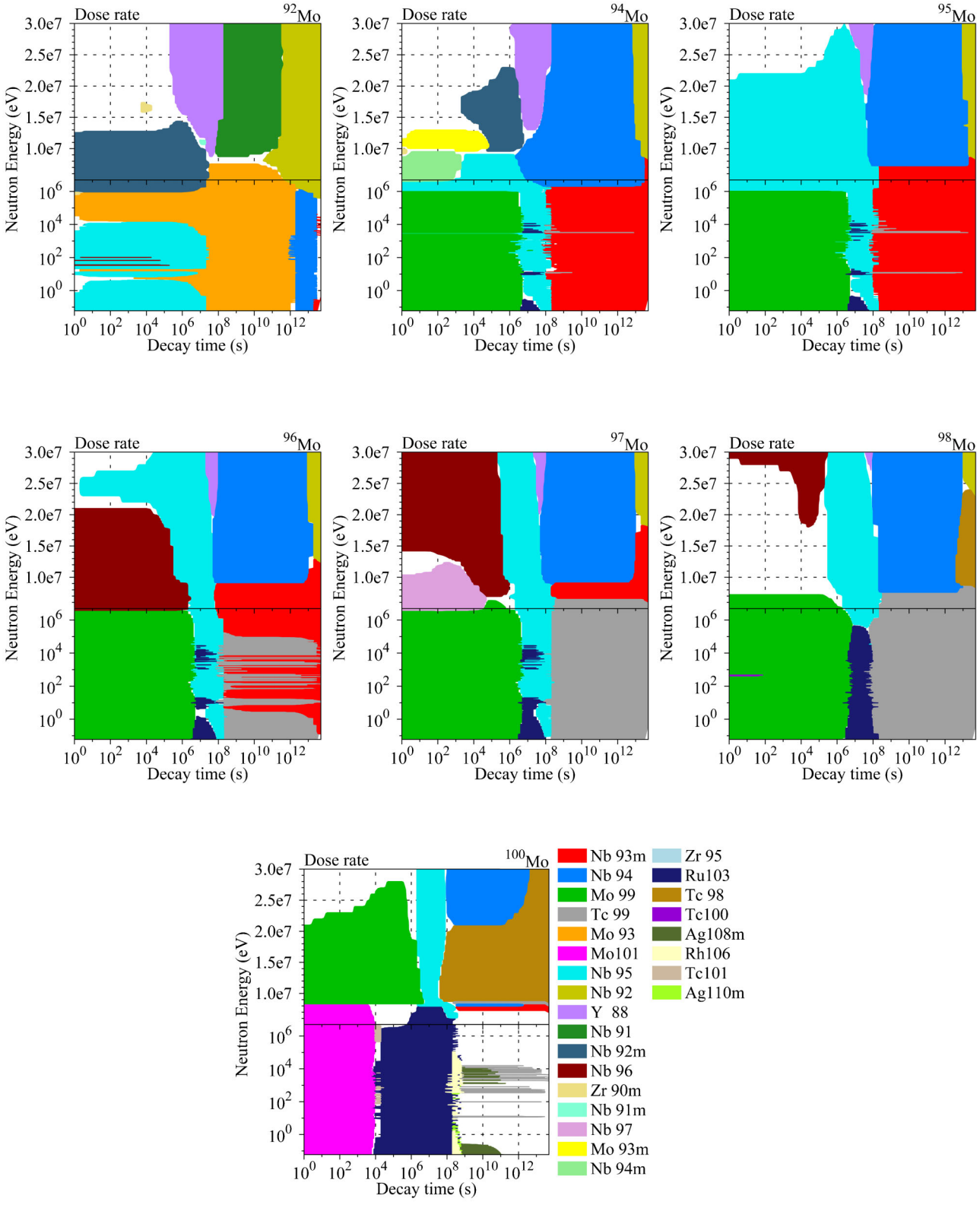

Fig. 11. Dose rate importance diagrams for the seven different naturally occurring isotopes of Mo after 5-yr irradiations at a flux of 1×10^{15} n·cm^{-2}·s^{-1}. In each case, 1 kg of the isotope (the isotope of each diagram is given at the top right-hand corner) was irradiated.

neutron energies, where the dominant regions of the overlapping nuclides appear in the ^{100}Mo diagram.

Unfortunately, since ^{94}Nb appears in all the importance diagrams and has large regions of dominance for many of the isotopes, it is unlikely that the activation problems of Mo can be completely negated. However, only the importance diagram for ^{92}Mo in Fig. 11 shows any significant region of dominance for ^{91}Nb, so removing this isotope from the chemical composition would certainly improve Mo's gamma dose rate activation response. Indeed, if the total dose rate is plotted with cooling time for each of the isotopes (and for natural Mo for comparison)—see Fig. 12—then the drop in the dose rate for ^{92}Mo beyond the 700-yr half-life of ^{91}Nb is obvious. Furthermore, the inventory calculations reveal that the amount of ^{94}Nb generated from ^{94}Mo and ^{95}Mo is much greater (at least two orders of magnitude higher) than from any other isotopes. In Fig. 12, this leads to a significantly higher dose rate for these two nuclides compared to the others (excluding ^{92}Mo) over a wide range of long cooling times.

Thus, isotopic tailoring of Mo, where the concentrations of ^{92}Mo, ^{94}Mo, and ^{95}Mo are removed or significantly reduced, could provide measurable improvements to the waste disposal prospects of Mo. Figure 12 suggests that on the 100-yr timescale, the gamma dose rate could be two orders of magnitude (or more) lower than in unaltered Mo, although this would still be markedly higher than in W or Fe (compare Figs. 9 and 12). Note that the best scenario for producing low activation Mo would be to use only ^{97}Mo because Fig. 12 indicates that it has by far the best activation response at long cooling times, although such extreme isotopic tailoring might be prohibitively expensive.

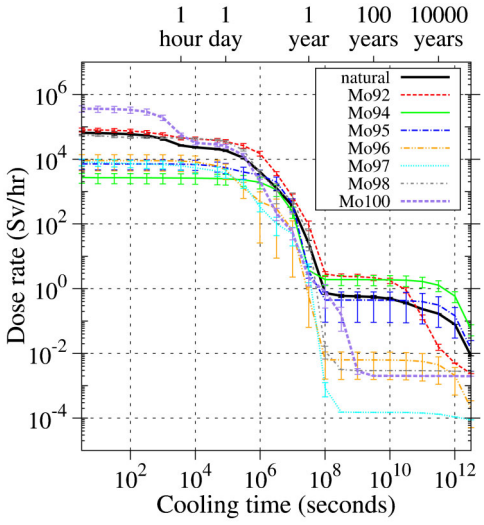

Fig. 12. The variation in dose rate during cooling after a 5-FPY irradiation of 1 kg of the different naturally occurring isotopes of Mo under a DEMO outboard equatorial first-wall armor spectrum with a total flux of 8.25×10^{14} n·cm^{-2}·s^{-1}. The results for naturally occurring Mo are also shown for comparison. The straight lines connecting adjacent data points serve as a guide to the eye only.

V. SUMMARY

In this paper we have presented two alternative visualization techniques for presenting the complex results generated by transmutation inventory calculations. First, we demonstrated the use of nuclide maps to display the time evolution in inventory composition (or contributions to a radiological quantity) under a specific neutron irradiation scenario. Such maps allow the large nuclide inventory generated during neutron-induced transmutation to be fully appreciated and also to observe how this inventory evolves in time. Additionally, inspecting the evolution in contributions to a specific radiological quantity during post-irradiation cooling can enable easy identification of the problematic radionuclides.

Second, the processing system used to generate importance diagrams[4] was updated, and this, together with the latest high-resolution nuclear data files, allows for much greater scope in the kinds of investigations that can be performed with these plots. Specifically, the efficient standardized processing approach means that parameter studies can be performed, where the varying quantity could be incident neutron flux, input material composition, or irradiation time.

Finally, the potential applications of these two techniques were illustrated by considering the contributions to gamma dose rate of the naturally occurring isotopes of Mo, and it was observed that Mo could become a more viable option for fusion if its composition were shifted toward the heavier end of its stable isotopic range.

ACKNOWLEDGMENTS

This work was partly funded by the Research Councils UK Energy Programme under grant EP/I501045 and the European Communities under the Contract of Association between EURATOM and Culham Centre for Fusion Energy.

REFERENCES

1. F. BROWN, B. KIEDROWSKI, and J. BULL, "MCNP5-1.60 Release Notes," LA-UR-10-06235, Los Alamos National Laboratory (2010); http://mcnp.lanl.gov/ (current as of Sep. 19, 2013).

2. X-5 MONTE CARLO TEAM, "MCNP—A General Monte Carlo N-Particle Transport Code, Version 5, Volume II: User's Guide," LA-CP-03-0245, Revision, Los Alamos National Laboratory (2008).

3. H. BATEMAN, "The Solution of a System of Differential Equations Occurring in the Theory of Radio-Active Transformations," *Proc. Cambridge Phil. Soc. Math. Phys. Sci.*, **15**, 423 (1910).

4. R. A. FORREST, "Importance Diagrams—A Novel Presentation of the Response of a Material to Neutron Irradiation," *Fusion Eng. Des.*, **43**, 209 (1998); http://dx.doi.org/10.1016/S0920-3796(98)00418-9.

5. J.-CH. SUBLET, J. W. EASTWOOD, and J. G. MORGAN, "The FISPACT-II User Manual," CCFE-R(11)11 Issue 4, Culham Centre for Fusion Energy (2013).

6. A. J. KONING et al., "TENDL-2012" (Jan. 11, 2013); ftp://ftp.nrg.eu/pub/www/talys/tendl2012/tendl2012.html (current as of Sep. 19, 2013).

7. A. J. KONIG and D. ROCHMAN, "Modern Nuclear Data Evaluation with the TALYS Code System," *Nuclear Data Sheets*, **113**, *12*, 2841 (2012); http://www.talys.eu/ (current as of Sep. 19, 2013); http://dx.doi.org/10.1016/j.nds.2012.11.002.

8. J.-CH. SUBLET, "The European Activation SYstem, EASY-II" (2013); http://www.ccfe.ac.uk/EASY.aspx (current as of Sep. 19, 2013).

9. M. R. GILBERT et al., "An Integrated Model for Materials in a Fusion Power Plant: Transmutation, Gas Production, and Helium Embrittlement Under Neutron Irradiation," *Nucl. Fusion*, **52**, 083019 (2012); http://dx.doi.org/10.1088/0029-5515/52/8/083019.

10. T. WILLIAMS and C. KELLEY, "Current Version of Gnuplot (4.6, patchlevel 4)" (2013); http://www.gnuplot.info/ (current as of Sep. 19, 2013).

11. R. A. FORREST et al., "Handbook of Activation Data Calculated Using EASY-2007," UKAEA FUS 552, UK Atomic Energy Authority (2009).

12. M. R. GILBERT and J.-CH. SUBLET, "Neutron-Induced Transmutation Effects in W and W-Alloys in a Fusion Environment," *Nucl. Fusion*, **51**, 043005 (2011); http://dx.doi.org/10.1088/0029-5515/51/4/043005.

13. M. J. LOUGHLIN and R. A. FORREST, "Comprehensive Activation Calculations of Reference Materials for Near Term Reactor Concepts," *Fusion Eng. Des.*, **69**, 711 (2003); http://dx.doi.org/10.1016/S0920-3796(03)00106-6.

14. J. HOW and R. REICHLE, "Plant Design Description," ITER-D-2X6K67 v1.0, ITER Baseline Document (2009).

15. *CRC Handbook of Chemistry and Physics*, 85th ed., D. R. LIDE, Ed., CRC Press, Boca Raton, Florida (2004).

16. J.-CH. SUBLET and G. J. BUTTERWORTH, "The Potential of Isotopic Tailoring for Titanium," *J. Nucl. Mater.*, **208**, 8 (1994); http://dx.doi.org/10.1016/0022-3115(94)90192-9.